Damage to monumental masonry buildings in Hatay and Osmaniye following the 2023 Turkey-Syria earthquakes: the role of wall geometry, construction quality and material properties

Baran Bozyigit[*1,2], Anil Ozdemir[3], Kokcan Donmez[4], Korhan Deniz Dalgic[5], Elif Durgut[6], Cennet Yesilyurt[5], Yavuz Dizgin[7], Canan Yıldeniz[8], Medine Ispir[6], Idris Bedirhanoglu[7], Yasemin Didem Aktas[4], Sinan Acikgoz[1]

[1]Department of Engineering Science, University of Oxford, Oxford, UK
[2]Department of Civil Engineering, Dokuz Eylul University, Izmir, Turkey
[3]Department of Civil Engineering, Gazi University, Ankara, Turkey
[4]Department of Civil, Environmental, and Geomatic Engineering, University College London, London, UK
[5]Department of Civil Engineering, Izmir Institute of Technology, Urla, Izmir, Turkey
[6]Department of Civil Engineering, Istanbul Technical University, Istanbul, Turkey
[7]Department of Civil Engineering, Dicle University, Diyarbakir, Turkey
[8]Chamber of Architects, Diyarbakir, Turkey

[*]Corresponding author: baran.bozyigit@deu.edu.tr

Abstract This paper reports on the findings of an investigation on 29 historic stone masonry buildings located in the cities of Hatay and Osmaniye following the recent Turkey-Syria earthquakes. The earthquake couplet on 6 February (with moment magnitudes 7.8 and 7.5) and the following aftershocks (including an event on 20 February with a moment magnitude of 6.3) resulted in significant damage to the buildings. To understand why, the examined buildings were assigned an EMS-98 damage level (ranging from 1 to 5) and descriptive response categories (masonry disaggregation, local mechanism and global response). Overall damage statistics indicated that masonry disaggregation was common and coterminous with local mechanism response. Wall geometry and construction quality indices were then investigated to explore why these were the dominant damage mechanisms. Wall geometry indices highlighted insufficient amount of walls to resist the local seismic demands, particularly in the transverse (e.g. short) direction of buildings. This deficit promoted the formation of local mechanisms. Construction quality indices suggested that stone layouts did not enable interlocking and that the walls were prone to disaggregation. To further investigate the role of material properties on the observed damage, materials were characterised using three non-destructive testing techniques: ultrasonic pulse velocity (UPV) measurements to estimate the static elastic modulus of stones, Schmidt rebound hammer (SRH) tests to estimate the compressive strength of stones, and the mortar penetrometer (MP) tests to estimate the compressive strength of mortar. The measurements indicated poor mortar quality, which may have expedited failures. Using established correlations, various other important material parameters (e.g. mortar cohesion and homogenised masonry strength) are derived. It is envisioned that the damage observations and the material measurements in this paper will inform detailed modelling efforts on the behaviour of historic masonry buildings during the 2023 Turkey-Syria earthquakes.

Keywords: Masonry, Earthquake damage, Wall geometry index, Masonry quality index, Non-destructive testing, Mortar penetrometer, Schmidt rebound hammer, Ultrasonic pulse velocity

1. Introduction

On 6 February 2023, at 04.17 and 13.24 (GMT+3 time zone), two earthquakes occurred in the province of Kahramanmaraş in Turkey. The first earthquake occurred at a depth of 10 km in Pazarcık and had a magnitude of M_w= 7.8. The second earthquake occurred at a depth of 10 km in Elbistan and had a magnitude of M_w=7.5. Thousands of aftershocks followed, including a major one on 20 February 2023, with the epicentre Uzunbağ in the Hatay province. It occurred at a depth of 16 km and had a magnitude of M_w= 6.3 (USGS, 2023). More than 50.000 people have lost their lives and 212.000 buildings were severely damaged or collapsed in the affected provinces (Karabacak et al., 2023). Fig.1a highlights the epicentres of these earthquakes.

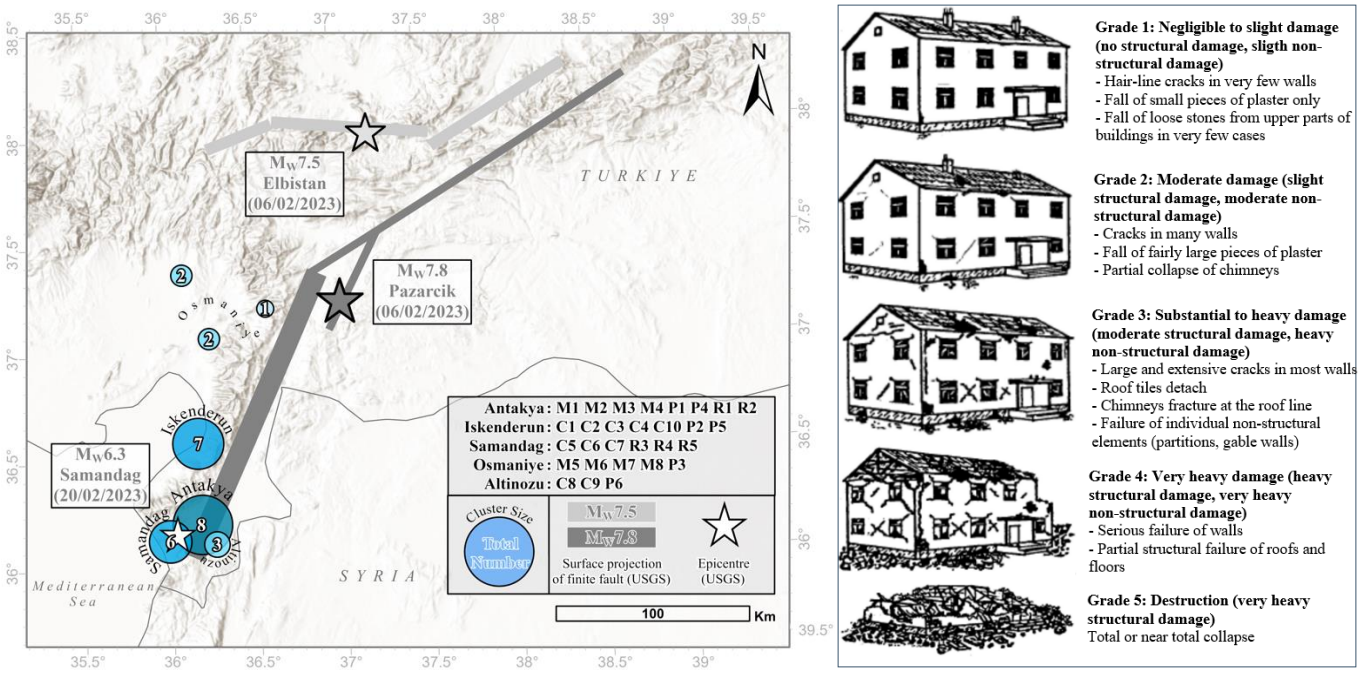

(a) (b)

Fig.1. a) Distribution of investigated buildings (see Table 1 for building IDs) with epicentres of Pazarcık and Samandağ earthquakes b) graphical representation and damage classification of masonry buildings according to EMS-98 (Grünthal and Levret, 1998)

The historic urban environments in the provinces of Hatay and Osmaniye were severely affected. Iconic buildings of worship, such as the Habib-i Neccar Mosque (Sanci, 2006), partially collapsed during the earthquakes. Historic public buildings, built during the 20th century French mandate of Hatay (Garbioğlu, 2017), were in use as local government or school buildings before the earthquakes. These buildings sustained severe damage. The large vernacular masonry building stocks in the districts of Antakya (Demir, 2016) and Samandağ (Sürmeli, 2019) featured examples of unique local architectural practice. Many of these buildings collapsed.

The architectonic characteristics of specific religious, public and residential buildings were investigated in the aforementioned studies. However, these studies do not provide enough information on the construction practices and materials to carry out engineering assessments. During the early part of 2010s, a major research project called SERAMAR characterised

the general features of vernacular masonry building stock in Antakya (Abrahamczyk et al., 2013). This comprehensive study included building surveys, material testing, building instrumentation, numerical modelling and risk mapping activities. However, detailed data regarding some components of this research (e.g. material testing data) is not publicly available. Regardless, amongst other contributions, the project highlighted observations regarding insufficient amount of walls and poor materials in vernacular masonry constructions in the region (Geneş et al., 2017).

After the 2023 Turkey-Syria earthquakes, several reconnaissance reports and post-earthquake studies have been published. Some of these reports emphasise the unique historical and architectural value of the historic structures in the region and present visual observations of damage patterns (EERC, 2023; TAÇDAM, 2023). The reports also highlight the need to repair (and where necessary strengthen) the monumental historic buildings that were damaged during the earthquakes. However, before the repair, retrofit and reconstruction activities are carried out, it is necessary to conduct scientific studies to understand the general reasons for damage. This paper presents an attempt to systematically categorise damage levels and types in monumental masonry structures and relate it to their wall geometry, construction quality and material properties. To achieve this, damage observations are quantified in Section 2. Section 3 and 4 investigate the potential role of geometric deficiencies (e.g. limited wall area) and poor construction quality (e.g. lack of interlocking in walls) in causing the damage. To do this, wall geometry indices (Lourenço et al., 2013) and masonry quality indices (Borri et al., 2015), are calculated for each building. Finally, Section 5 presents the non-destructive measurements conducted to quantify the material properties in the historic buildings. The transformation of damage observations, geometry, construction quality and material characteristics into quantifiable parameters enables a systematic evaluation of the correlations between these aspects. Section 6 summarises the correlation trends to establish some of the key causes of damage. This section also highlights the limitations of the indices and presents a brief discussion on how they can be improved.

2. Building damage survey

In the two field studies performed by the authors between 13.03.23-20.03.23 and 11.04.23-21.04.23, 29 stone masonry buildings consisting of 10 churches, 8 mosques, 6 public and 5 residential buildings were investigated. All the examined buildings were constructed using unreinforced masonry and did not include metal reinforcements or timber tie beams (except for one building where sporadic timber tie beam use was noted but judged ineffective). The buildings were chosen as they represent monumental examples of the unique architectural heritage of the region. The investigated structures are associated with an ID and province in Table 1. The examined buildings are from the Mamluk, Ottoman, French Mandate and Early Turkish Republic periods. Specific dates of construction are not reported due to uncertainties in the architectural and historical resources examined by the authors. Due to frequent seismic events in the area, many of the examined buildings underwent periodic repair, retrofit and reconstruction activities, the extent of which is unclear. The last major earthquakes in the region date to the second half of the 19th century (Över et al., 2011); historical records suggest that existing buildings may have been subjected to substantial

repairs during that time. The original timber floors of four some buildings (M5, P1-P4) were replaced with reinforced concrete slabs during more recent works.

To evaluate the local seismic demand, each building is associated to the nearest strong-motion station with available data (AFAD, 2023). Only the records from the Pazarcık main shock and Uzunbağ aftershock were considered since the Elbistan event was far away from the investigated structures (Fig.1a). Preliminary damage level classification of buildings is conducted using the five EMS-98 damage grades (DGs) which range from negligible damage to total collapse (Mavroulis et al., 2019). Fig. 1b presents a graphical representation of damage classes and their description. To avoid ambiguity, EMS-98 classification was only conducted on the main walls of the structures. Non-structural walls (e.g. parapets), floor and roof systems (e.g. domes, vaults) and annexed structures (minarets, towers and porches) are not considered in the DG assignment. Figs.3a-e show the location of the investigated buildings in Iskenderun, Antakya, Samandağ, Altınözü (districts of Hatay) and Osmaniye. On the maps, building types are indicated with symbols and coloured according to the building DGs. General photographs of the buildings are presented alongside detailed damage photographs.

Table 1. ID, name, type and province of investigated historic masonry buildings associated with the nearest strong-motion stations

ID	Building Name	Type	Province	Main shock		Aftershock	
				6 February 2023 (M_w=7.8)		20 February 2023 (M_w=6.3)	
				Station	Distance (km)	Station	Distance (km)
C1	Surp Karasun Manuk Church	Church	Hatay	3115	4.4	3119	1.4
C2	St. Nicholas Orthodox Church	Church	Hatay	3115	4.2	3119	1.3
C3	Latin Catholic Church	Church	Hatay	3115	4.5	3119	1.6
C4	Syriac Catholic Church	Church	Hatay	3115	4.4	3119	1.4
C5	Batıayaz Armenian Church	Church	Hatay	3140	9.4	3140	9.4
C6	The Virgin Mary Samandağ Orthodox Church	Church	Hatay	3140	4.6	3140	4.6
C7	St. Ilyas Orthodox Church	Church	Hatay	3140	4.5	3140	4.5
C8	St George Sarılar Orthodox Church	Church	Hatay	3136	0.8	3136	0.8
C9	The Virgin Mary Tokaçlı Orthodox Church	Church	Hatay	3136	1.9	3136	1.9
C10	St George Iskenderun Orthodox Church	Church	Hatay	3115	3.5	3119	0.7
M1	Habib-i Neccar Mosque	Mosque	Hatay	3132	0.8	3124	3.8
M2	Sarımiye Mosque	Mosque	Hatay	3131	0.9	3124	4.0
M3	Şeyh Ali Mosque	Mosque	Hatay	3132	0.6	3124	3.7
M4	Kurşunlu Han Mosque	Mosque	Hatay	3132	0.9	3124	3.7
M5	Enverül Hamit Mosque	Mosque	Osmaniye	8003	2.1	8003	2.1
M6	Ağcabey Mosque	Mosque	Osmaniye	8002	2.4	2709	11.6
M7	Ala Mosque	Mosque	Osmaniye	8004	0.9	8004	0.9
M8	Hamidiye Mosque	Mosque	Osmaniye	8004	0.7	8004	0.7
P1	Hatay Metropolitan Municipality Building	Public	Hatay	3123	1.2	3124	3.8
P2	Mithatpaşa Primary School	Public	Hatay	3115	4.5	3119	1.6

P3	Yedi Ocak Primary School	Public	Osmaniye	8003	2.2	8003	2.2
P4	Antakya High School	Public	Hatay	3123	1.1	3124	3.9
P5	Iskenderun High School	Public	Hatay	3115	4.0	3119	1.1
P6	Olive Museum	Public	Hatay	3136	2.0	3136	2.0
R1	Gali Mansion-I	Residential	Hatay	3132	0.4	3124	3.6
R2	Gali Mansion-II	Residential	Hatay	3132	0.4	3124	3.6
R3	Hıdırbey Gastronomy House	Residential	Hatay	3140	5.3	3140	5.3
R4	Vakıflı No.2 House	Residential	Hatay	3140	4.2	3140	4.2
R5	Old English School	Residential	Hatay	3140	4.0	3140	4.0

EMS-98 DGs provide an indication of damage level. To discuss the types of damage encountered in the field, another classification (Borri et al., 2020) is useful. In this classification, masonry building response is classified under three categories: i) masonry disaggregation, ii) local response, and iii) global response. Masonry disaggregation refers to the detachment of masonry units and mortar when subjected to strong ground motions. It is generally observed when weak mortar is used alongside irregular small stones (see Figs.2a-b). The second classification, local response, refers to the presence of mechanisms featuring one or more structural components. It generally involves out-of-plane motion. For instance, the overturning of the entire façade (e.g. C4 in Fig. 3a) or the first storey walls and the roof of a building in its transverse (e.g. short) direction (e.g. P2 in Fig. 3a) are classified as local response. The third classification, global response, is expected for structures with good construction quality and effective load transfer between masonry walls. Global response classification implies in-plane damage, such as flexural and shear cracking, concentrated around wall openings (e.g. P1 in Fig.3b, M5 in Fig.3e). The absence of visible structural damage in the walls was taken as global response (e.g. C1 in Fig. 3a, C5 in Fig. 3c).

For the buildings examined, multiple response types had to be assigned as disaggregation was often observed alongside local or global response mechanisms. Fig.2a shows an instance where a local response mechanism involving the separation of building façades is seen alongside disaggregation. In Fig. 2b, the upper part of the disaggregated and leaning wall appears to have initiated a local response leading to vault collapse due to spreading supports. The EMS-98 DG and building response type are listed in Table 2.

(a) (b)

Fig.2 Partially disaggregated masonry walls and local response mechanisms from a) R1 and b) C8.

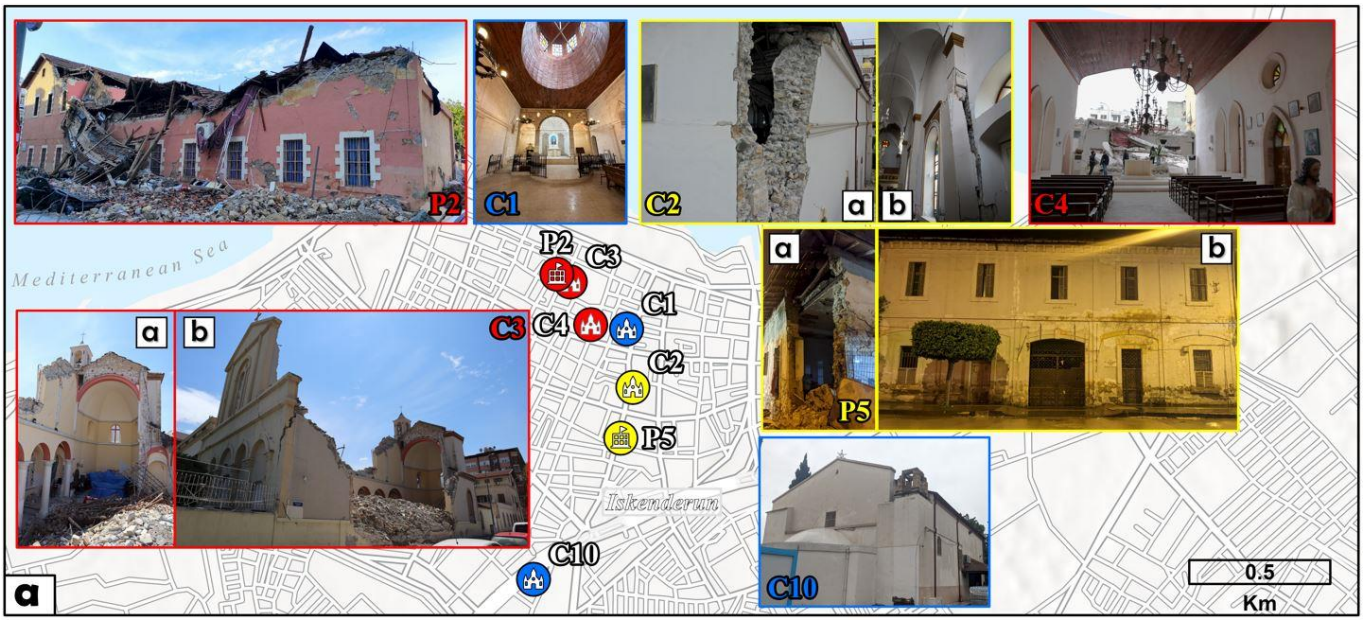
P2
C1
C2
a
b
C4
Mediterranean Sea
P2
C3
C1
C4
C3
C2
P5
Iskenderun
C10
a
b
P5
C10
0.5
Km

123

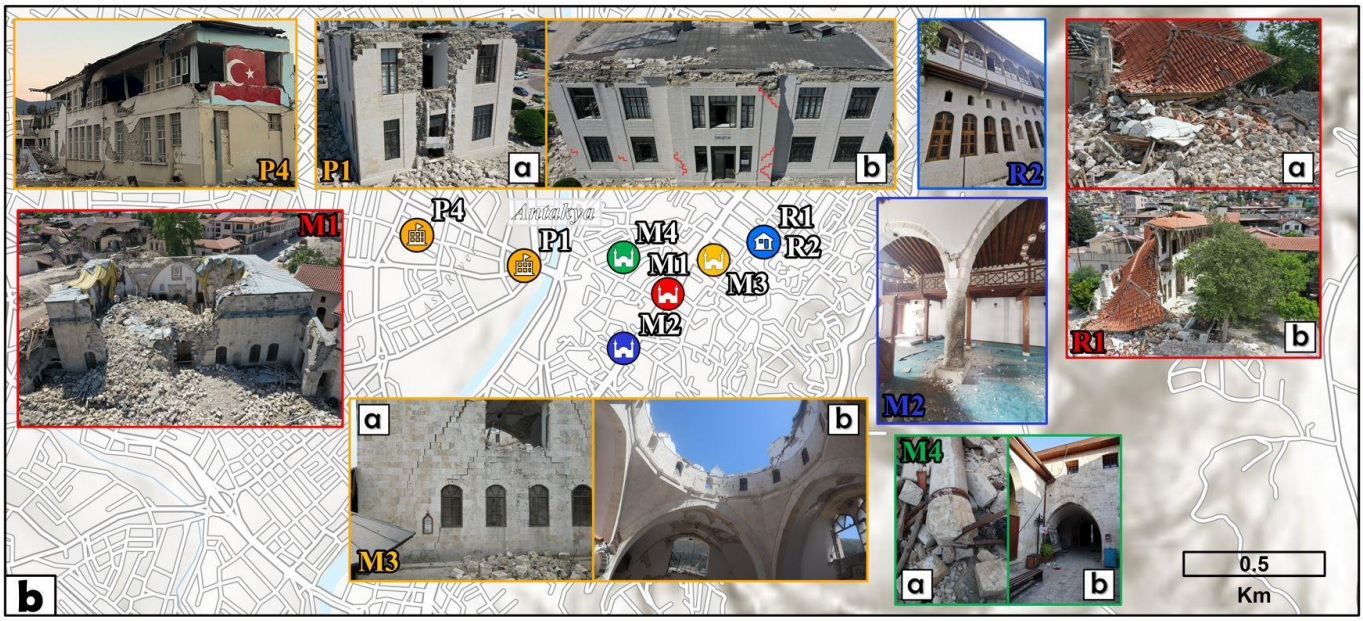
P4
P1
a
b
R2
a
M1
P4
Antakya
P1
M4
M1
M3
M2
R1
R2
M2
R1
b
a
b
M3
M4
a
b
0.5
Km

124

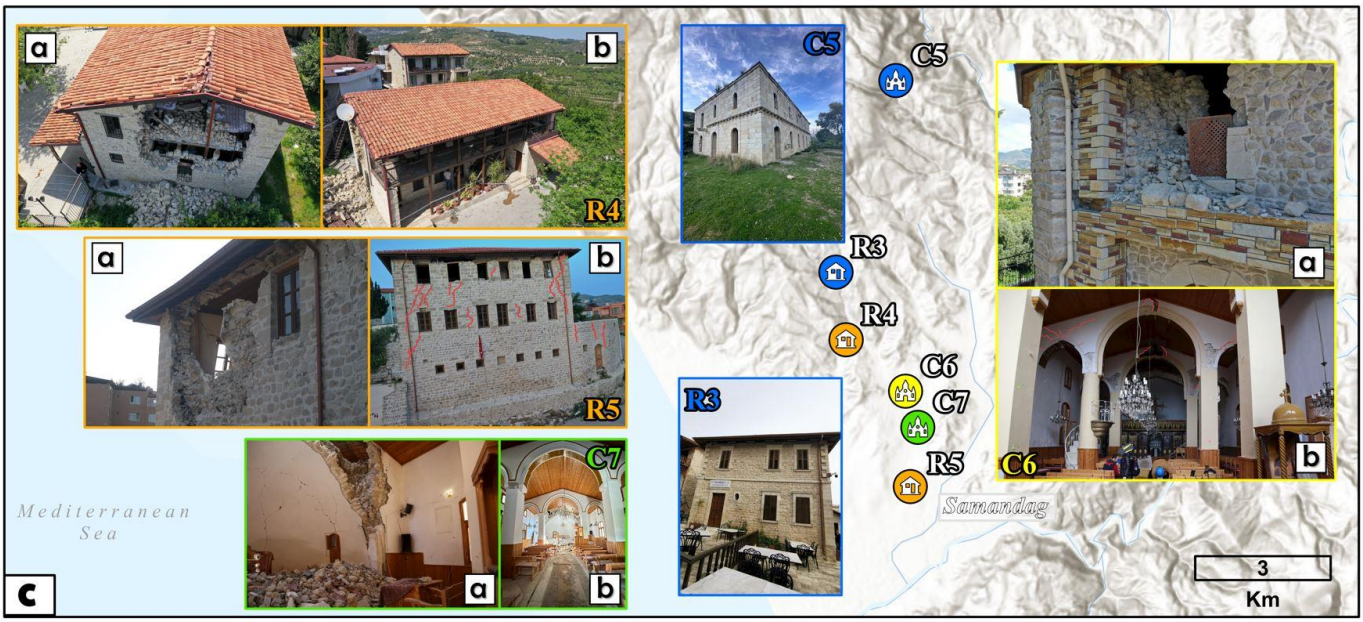
a
b
R4
a
b
R5
C7
a
b
Mediterranean Sea
C5
C5
R3
R4
C6
C7
R5
R3
Samandag
a
C6
b
3
Km

125

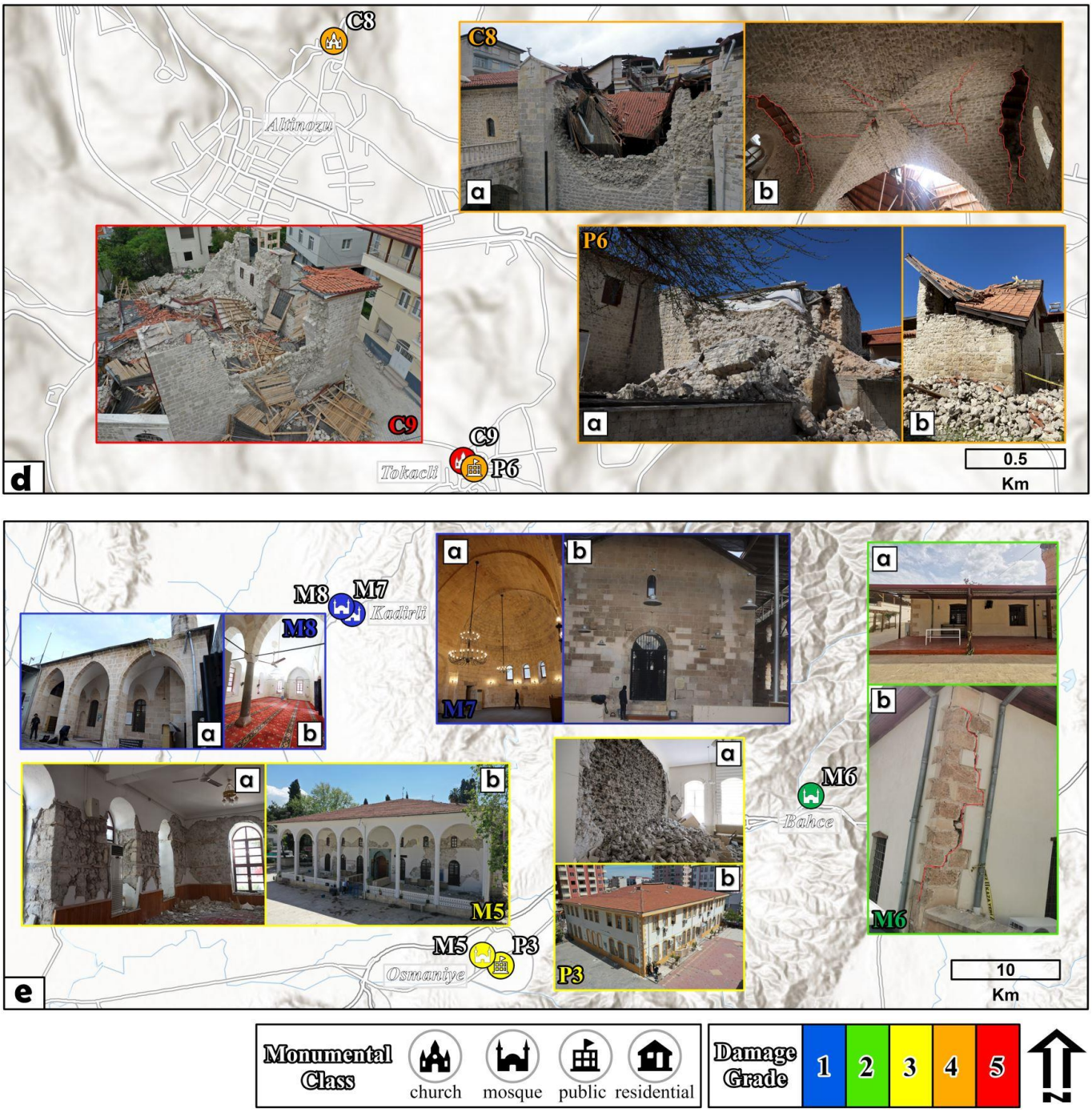

Fig.3. Location, EMS-98 DGs and photographs of the investigated buildings from (a) Iskenderun (b) Antakya c) Samandağ d) Altınözü e) Osmaniye

To aid damage evaluation, Table 2 also presents the resultant peak ground acceleration (PGA) values from the stations listed in Table 1 for the 6 February main shock and the 20 February aftershock. The resultant PGA values are obtained by processing the N-S and E-W acceleration records (Banerjee Basu and Shinozuka, 2011). Table 2 indicates that the largest PGA was 0.66*g* and recorded in the district of Antakya on the 6th of February. This is consistent with the USGS surface fault rupture map in Fig. 1, which indicates that the district of Antakya lies on the fault rupture footprint. Preliminary investigation reports (Taftsoglou et al., 2023; Ozturk et al., 2023) suggest that ground motion within Antakya varied significantly due to local site conditions and basin effects; this is reflected in the range of PGA values, 0.42-0.66*g* in Table 2, recorded in this district. Noteworthy vertical

accelerations were also recorded in Antakya (Sagbas et al., 2023) and may have had a significant influence on structural behaviour; however, this aspect remains outside the scope of this first investigation. The resultant PGA magnitudes for the other districts are ordered from the largest to smallest as follows: Altınözü, İskenderun, Bahçe, Samandağ, Kadirli and Merkez. The 20 February aftershock was located close to the districts of Antakya, Altınözü and Samandağ (listed in decreasing order of resultant PGAs) and caused resultant peak accelerations exceeding 0.2*g*. Partial collapses of several buildings in these districts (e.g. C7 and R4 in Fig.3c) reportedly occurred during the aftershock. However, since the damage assessments were conducted after the aftershock, progressive evaluation of damage is not possible. In the following, the larger of the resultant PGAs from the main and aftershock will be considered representative of the seismic demand.

Table 2. Seismic response type (Borri et al., 2020) and damage classification of buildings with resultant PGA values

Building (wall construction)	District	Resultant PGA (g)		Response type			DG (EMS-98)
		6 February 2023 (M_w=7.8)	20 February 2023 (M_w=6.3)	Disaggregation	Local	Global	
C1 (RSM)	İskenderun	0.33	0.12			X	DG1
C2 (ISM)	İskenderun	0.33	0.12	X	X		DG3
C3 (RSM)	İskenderun	0.33	0.12	X	X		DG5
C4 (ISM)	İskenderun	0.33	0.12		X		DG5
C5 (RSM)	Samandağ	0.26	0.22			X	DG1
C6 (ISM)	Samandağ	0.26	0.22	X	X		DG3
C7 (ISM)	Samandağ	0.26	0.22	X	X		DG2
C8 (ISM)	Altınözü	0.54	0.33	X	X		DG4
C9 (ISM)	Altınözü	0.54	0.33	X	X		DG5
C10 (n/a)	İskenderun	0.33	0.12			X	DG1
M1 (RSM)	Antakya	0.58	0.54	X	X		DG5
M2 (RSM)	Antakya	0.42	0.54			X	DG1
M3 (RSM)	Antakya	0.58	0.54	X	X		DG4
M4 (RSM)	Antakya	0.58	0.54	X		X	DG2
M5 (ISM)	Merkez	0.19	0.04	X		X	DG3
M6 (RSM)	Bahçe	0.29	0.02		X		DG2
M7 (RSM)	Kadirli	0.20	0.01			X	DG1
M8 (RSM)	Kadirli	0.20	0.01			X	DG1
P1 (RSM)	Antakya	0.66	0.54	X		X	DG3
P2 (ISM)	İskenderun	0.33	0.12	X	X		DG5
P3 (ISM)	Merkez	0.19	0.04	X		X	DG3
P4 (RSM)	Antakya	0.66	0.54	X		X	DG4
P5 (ISM)	İskenderun	0.33	0.12	X		X	DG3
P6 (RSM)	Altınözü	0.54	0.33	X	X		DG4
R1 (RSM)	Antakya	0.58	0.54	X	X		DG5
R2 (RSM)	Antakya	0.58	0.54	X		X	DG1
R3 (RSM)	Samandağ	0.26	0.22		X		DG1
R4 (RSM)	Samandağ	0.26	0.22	X	X		DG4
R5 (RSM)	Samandağ	0.26	0.22	X		X	DG4
Incidence of response type (%)				~70	~50	~50	

146 The first column of Table 2 broadly specifies the wall construction technique (i.e. whether the external wall is faced with
147 Regular Stone Masonry (RSM) or Irregular Stone Masonry (ISM)), while the last row summarises the incidence of response
148 type. Masonry disaggregation was observed in 70% of the investigated buildings and in almost all of the ISM walls. Half of the
149 buildings featured crack patterns indicative of the formation of local mechanisms (50%) – most of these also experienced
150 disaggregation. Global response with box-like behaviour was observed in 50% of the investigated buildings; these buildings
151 either featured in-plane flexural and shear cracks or no visible damage. Floor structures in some of these buildings (M5, P1 and
152 P3) were either reconstructed or retrofitted with reinforced concrete slabs, which ensured diaphragm action and confined the
153 response to in-plane mechanisms. Some buildings with timber floor structures (e.g. R2 and R5) also experienced global response.
154 The damage survey presented in this section indicates that masonry disaggregation was commonly observed, often alongside
155 the formation of local response mechanisms. To better understand the potential reasons for these dominant mechanisms, the next
156 section explores wall geometry indices.

157 **3. Wall geometry assessment**

158 The wall geometry indices or simplified seismic indices (Lourenço et al., 2013; Lourenço and Roque, 2006) were established
159 to screen the damage vulnerability of monumental masonry buildings. These indices use wall geometry and local PGA
160 information to judge if a structure is 'safe' or 'unsafe'. They were formulated for large span monumental masonry structures and
161 their performance was evaluated using data from damage to monumental buildings in Europe and New Zealand. In this paper,
162 geometry indices are used as a diagnostic tool to establish the potential role of geometric aspects on damage.
163 There are two sets of indexes: in-plane and out-of-plane. In-plane indices are useful to understand whether the building has
164 enough walls to carry the horizontal seismic loads in-plane in each direction. If the amount of walls are insufficient, local
165 mechanisms involving out-of-plane motion of structural components may be initiated. Out-of-plane indices evaluate the stability
166 of walls against overturning failure. Thresholds define safe-unsafe boundaries; the safe classification indicates buildings which
167 are safe to enter after an earthquake. This should correspond to DG3 or lower damage levels.
168 The first in-plane index is the ratio of the plan area of walls in one main direction of the building to the total plan area of the
169 building. Eurocode 8 suggests a minimum safe value of 5-6% for regular structures with rigid diaphragms while 10% is
170 recommended for historic masonry buildings located in high seismicity regions. Lourenço et al.'s (2013) suggestion to adopt a
171 safety threshold of 10% for PGA's up to 0.25g and a linear increase for higher PGA's is followed in this study. Eqs. (1) are used
172 to calculate the first in-plane index for the transverse (x) and longitudinal (y) directions:

173 $$\lambda_{i1x} = \frac{A_{wx}}{A_{plan}}, \lambda_{i1y} = \frac{A_{wy}}{A_{plan}} \quad (1)$$

174 where λ_{i1} is the first in-plane index, A_w refers to the plan area of earthquake resistant walls (in either x or y direction, as indicated
175 in the subscript), and A_{plan} is the total plan area of the building.

The second in-plane index is the base shear ratio. It is the ratio of shear resistance of the building to the shear demand in each main direction. Assuming zero cohesion and self-weight, the base shear ratio can be calculated using Eq.(2) (Lourenço et al., 2013). Due to the rectangular plan geometry of the investigated buildings, A_{wy} is typically high when compared to A_{wx}. Therefore the second in-plane index will be calculated only for the x direction:

$$\lambda_{i2} = \frac{\mu A_{wx}}{\left(A_{wx} + A_{wy}\right)\beta} \tag{2}$$

where λ_{i2} is the second in-plane index, μ is the coefficient of friction (assumed as 0.4 according to Eurocode 6 (2005)) and β is an equivalent seismic static coefficient (taken conservatively as the higher of the resultant PGA's from the main shock and aftershock in Table 2). λ_{i2} values smaller than 1 indicate unsafe conditions where the demand is higher than the resistance.

The geometric ratio of thickness to height of masonry walls is used as the out-of-plane index λ_o (Lourenço et al., 2013):

$$\lambda_o = \frac{t_w}{h_w} \tag{3}$$

where t_w is the wall thickness and h_w is the average height of wall. Minimum values of λ_o are considered if there are different geometric configurations for walls in the same building. The slenderness ratio in Eq.(3) corresponds to the pseudo-static load capacity of an unachored rigid rectangular block (Housner, 1963); if evaluated conservatively, it may indicate the PGA required to overturn the wall. However, Lourenço et al. (2013) suggested less conservative thresholds for the out-of-plane indexes using empirical observations. These are adopted in the current study.

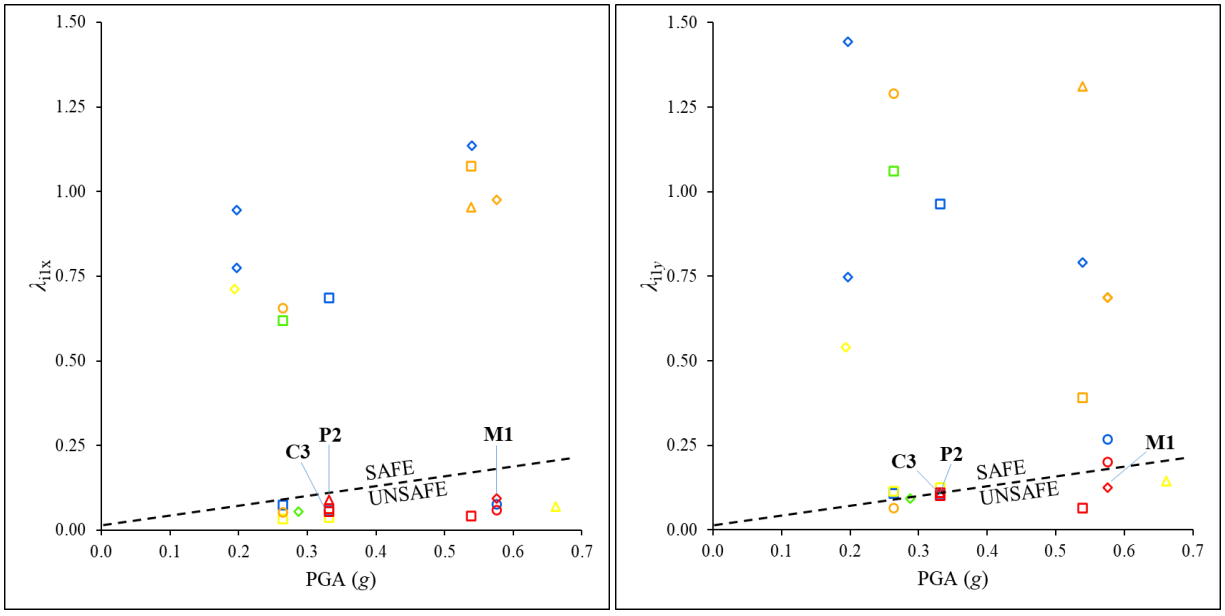

(a) (b)

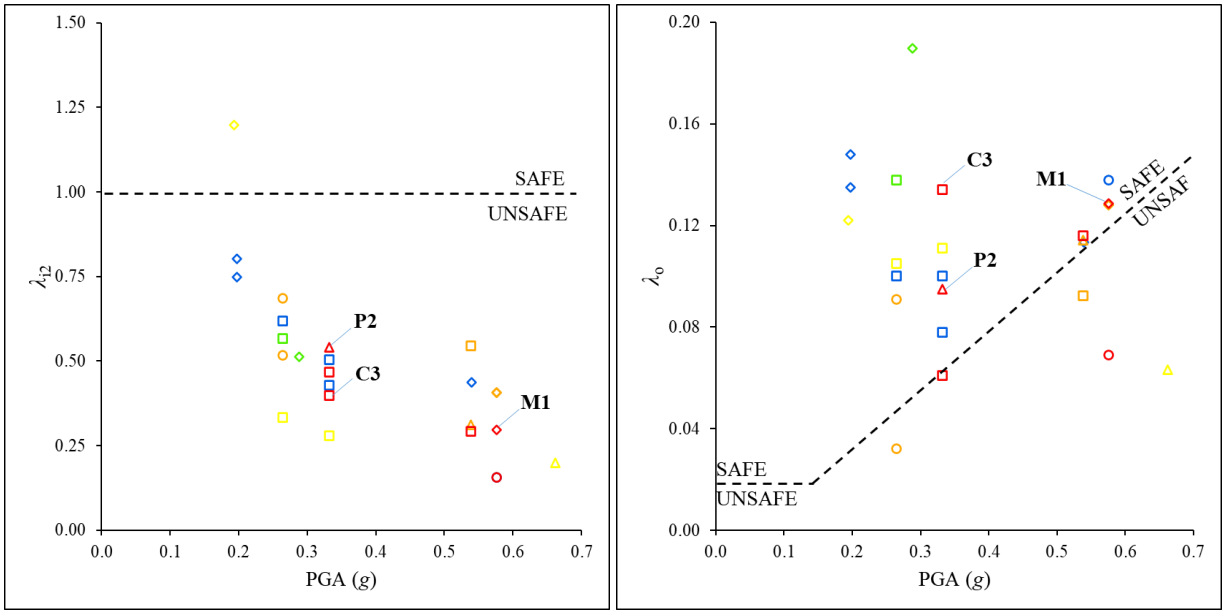

(c) (d)

Fig.4. Relationship between a) λ_{i1x} and PGA b) λ_{i1y} and PGA c) λ_{i2} and PGA d) λ_o and PGA (□: church, ◊: mosque, Δ:public, ○: residential, blue: DG1, green: DG2, yellow: DG3, orange: DG4, red: DG5 according to EMS-98)

Drawings of only some of the examined structures were available and were used to determine the geometric parameters required to calculate the indices. For structures without drawings, laser scanning and photogrammetry data collected during the post-earthquake field work were processed to extract the required parameters. Figs.4a-b show the relationship between λ_{i1} in x and y directions and PGA. In these figures, markers indicate the data from individual buildings, where the marker type indicates building category (e.g. square markers refer to churches). The markers are colour coded with reference to their DGs. According to Figs.4a-b, ~42% of the buildings are unsafe according to λ_{i1x} in the transverse direction, ~38% of the buildings are unsafe according λ_{i1y} in the longitudinal direction. The differences between these index results from the two directions are due to the typically larger plan area of walls in the longitudinal direction of buildings.

The results for the second in-plane index in the transverse direction in Fig.4c indicate that only one building is in the safe region. All buildings with DG levels 1 and 2 are located in unsafe areas. This indicates that in its current form, the second in-plane index in-plane provides a conservative assessment of safety. This is to be expected since important factors such as the contribution of material resistance (due to cohesion and tensile capacity) and other load distribution systems (such as rigid diaphragms, see concrete floors in P1 Fig.3b, or transverse arched frames in church naves, see C6 in Fig.3c) are neglected in the index calculations. However, the large percentage of unsafe classifications in the in-plane indices highlight a potential deficit for the examined structures in terms of their wall area to resist the earthquakes. The fact that all collapsed structures (DG5) are located in the unsafe regions of Figs.4a-c corroborates this statement.

As mentioned earlier, insufficient in-plane resistance in the transverse direction may lead to the formation of local mechanisms involving out-of-plane motion of structural components. The collapse of the structures rated DG5 in Table 2

(including C3, M1 and P2) was due to local mechanism formation and out-of-plane motion of walls in the building transverse direction (see Fig. 3). To evaluate the vulnerability of walls to overturning instability during out-of-plane motion, Fig.4d explores the relationship between λ_o and PGA. According to Fig.4d, only 5 of the buildings have unsafe walls, indicating that the walls of structures were, in general, sufficiently thick to prevent out of plane instability. However, several building walls in the safe zone of Fig.4d (including C3, M1 and P2) collapsed in the out-of-plane direction.

Overall, the in-plane indices indicate insufficient amount of walls, especially in the building transverse direction. This deficit may partially explain the formation of local mechanisms for many of the examined structures. The out-of-plane index suggests that walls were sufficiently thick to prevent overturning instabilities. This contradicts the damage survey observations in Section 2, where multiple collapse cases due to out-of-plane action were noted. This apparent contradiction is related to the poor construction quality of walls, which led to disaggregation and significantly reduced their out of plane capacity. This aspect is investigated next.

4. Construction quality evaluation

Masonry disaggregation under horizontal seismic actions is one of the main reasons for out-of-plane damage in thick masonry walls. A qualitative index called Masonry Quality Index (MQI) was proposed in (Borri et al., 2015) to account for the quality of masonry constructions in historic masonry buildings. Borri et al. (2020) relate the index values to the expected masonry failure modes. For instance, poor quality masonry walls with a low MQI are considered prone to disaggregation as a result of out-of-plane actions. To understand if poor masonry construction quality is the cause of disaggregation for the structures in Table 2, this section investigates their MQI.

To calculate MQI, the conservation state (*SM*), stone dimensions (*SD*), stone shapes (*SS*), wall leaf connections (*WC*), mortar joint geometry (*HJ* and *VJ*), and mortar quality (*MM*) parameters are evaluated. For each parameter, one of the following grades is given: F (fulfilled), PF (partially fulfilled) and NF (not fulfilled). MQI is then calculated using a simple formula which weighs parameters according to their importance for the given loading scenario. In this paper, only MQI of walls under horizontal out-of-plane actions is calculated:

$$MQI = SM\left(SD + SS + WC + HJ + VJ + MM\right) \tag{4}$$

where *MQI* represents the masonry quality index value for horizontal out-of-plane action. The numerical values of the parameters required to calculate MQI under a given action, for a chosen fulfilment level (NF, PF or F) are provided in Table 3 and the fulfilment criteria are discussed next.

Table 3. Numerical values of the parameters (*SM*, *SD*, *SS*, *WC*, *HJ*, *VJ* and *MM*) used to calculate MQI under horizontal out-of-plane actions for various fulfilment levels (NF, PF and F) (Borri et al., 2020)

	MQI		
Parameter	NF	PF	F

SM	0.5	0.7	1
SD	0	0.5	1
SS	0	1	2
WC	0	1.5	3
HJ	0	1	2
VJ	0	0.5	1
MM	0	0.5	1

Fig.5. Representative zoom-in views of typical walls investigated in Table 6

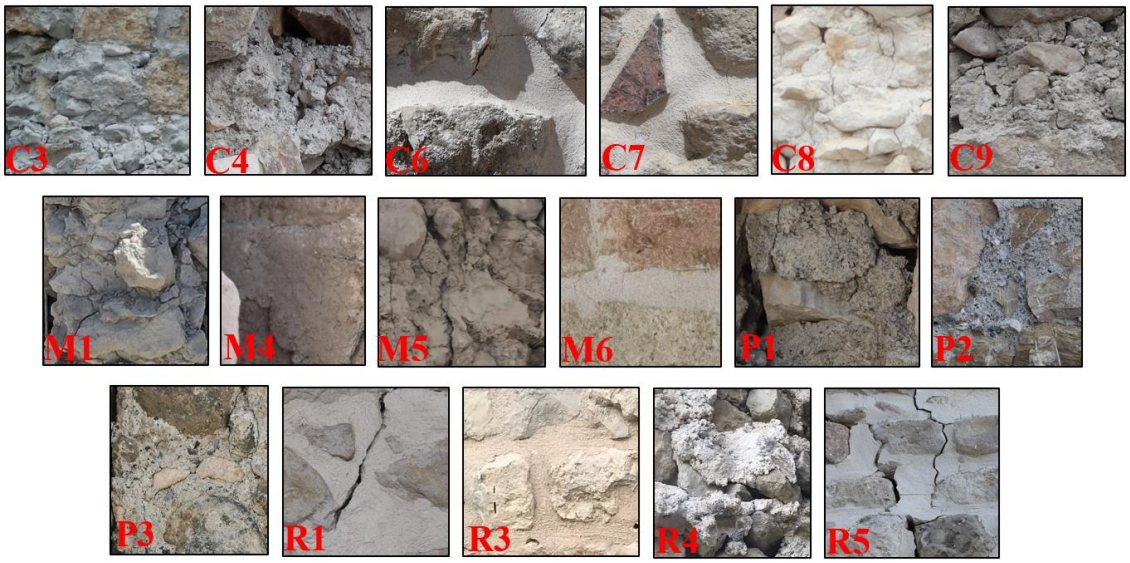

Fig.6. Representative zoom-in views of mortars investigated in Table 7

The fulfilment criteria for most MQI parameters are evaluated visually. For instance, the parameter *SS* refers to the shape of stonework. Representative cross-sections of walls and general view of mortars are shown in Figs.5-6, respectively. These indicate

a wide variety of materials and construction techniques. ISM walls do not satisfy the fulfilment criteria for SS and are graded NF. RSM walls may be composed of cut stones through their thickness or may have distinct leaves. In Multi-Leaf Masonry (MLM) walls, the building external façade is often faced with cut-stones. If there is only one masonry leaf with cut stone, the grade PF is given. If both external leaves are made of cut stone, the grade F is given. Separately, the quality of mortar parameter *MM* is also evaluated visually, however, this evaluation is more subjective. It aims to classify the conservation state, strength, and regularity of mortar with a single parameter. In this classification, mortar in ISM walls is rated NF or PF. In MLM walls mortar is rated PF or F. In both cases, if the mortar is crumbly, the lower fulfilment level is chosen.

(a) (b) (c)

Fig.7. a) Stone dimension measurements from a point cloud (Building: C5), b) photograph of a through thickness cross-section of a disaggregated wall used for *WC* calculation (Building: M1), and c) an exposed wall surface used for *VJ* calculation (Building: C3)

Geometric measurements may be conducted to evaluate fulfilment criteria for some of the MQI parameters. For instance, the parameter *SD* refers to stone dimensions in the wall. The fulfilment criterion for this parameter is the presence of more than 50% of stones with length greater than 40 cm. *SD* can be calculated using individual stone size measurements from laser scan or photogrammetry point clouds (see Fig.7a). Another parameter that can be calculated qualitatively from point clouds or orthoimages is *WC*; this calculation requires exposed through-thickness wall cross-sections. First, the distance between two points in vertical direction is measured (see L_v in Fig.7b). Then, for the same points, the length of the shortest connection path through mortar joints (see L_m in Fig.7b) is measured. *WC* fulfilment category is determined using the ratio of L_m to L_v (e.g. the criteria is F if $L_m/L_v > 1.6$). Another quantitative measurement option is available for the parameter of *VJ*, which can be evaluated from exposed masonry surfaces on the façade (see Fig.7c). The fulfilment category for *VJ* is F if $L_m/L_v > 1.6$. In this paper, the quantitative approaches were adopted whenever data was available. Otherwise, the qualitative approach was used following (Borri et al., 2015; Borri et al., 2020).

Once all the parameters are determined, Eq.(4) is used to calculate the *MQI*. The final value of *MQI* is used to assign the wall a quality category (*A*, *B* and *C*): $0 \leq MQI \leq 4$ is Category "*C"*, poor quality, $4 \leq MQI \leq 7$ is Category "*B*", average quality, and $7 \leq MQI \leq 10$ is Category "*A*", good quality. According to Borri et al. (2020), all Category "*C"* walls are prone to disaggregation.

Table 4 specifies the wall constructions broadly as ISM or RSM and presents the MQI classifications of 19 buildings where exposed masonry surfaces and/or through thickness cross-sections were available to enable the aforementioned parametric evaluations. The presence of disaggregation (obtained from Table 2) and the safety classification of the walls from the out of plane index λ_o (obtained from Fig. 4d) are also indicated in Table 4. The colour coding in Table 4 (e.g. red, yellow and green font colours) is provided to evaluate correlations between MQI category, disaggregation response and the λ_o safety index. All buildings constructed with ISM are in category "*C"*. This implies that masonry disaggregation is expected for this type of wall construction under horizontal seismic action. According to Table 4, all Category "*C*" buildings except C4 experienced masonry disaggregation. Some Category "*B*" buildings (M1, M3 and R1) also experienced masonry disaggregation. It should be noted that the wall internal connection criteria *WC* is not fulfilled ("NF") for these buildings.

Table 4. MQI values and categories of buildings according to horizontal out-of-plane loading condition with λ_o and disaggregation evaluation

Building	Wall construction	*MQI*	Category	Out-of-plane seismic index (λ_o) safety criteria	Disaggregation
C2	ISM	1	*C*	Safe	Yes
C3	RSM	2.8	*C*	Safe	Yes
C4	ISM	1.4	*C*	Unsafe	No
C5	RSM	6	*B*	Safe	No
C6	ISM	0.35	*C*	Safe	Yes
C7	ISM	0.5	*C*	Safe	Yes
C8	ISM	1.4	*C*	Unsafe	Yes
C9	ISM	1.05	*C*	Safe	Yes
M1	RSM	6.5	*B*	Safe	Yes
M3	RSM	5.5	*B*	Safe	Yes
M5	ISM	1	*C*	Safe	Yes
P1	RSM	0.35	*C*	Unsafe	Yes
P2	ISM	0.7	*C*	Safe	Yes
P3	ISM	1	*C*	n/a	Yes
P5	ISM	0.7	*C*	n/a	Yes
P6	RSM	2.1	*C*	Safe	Yes
R1	RSM	5.5	*B*	Unsafe	Yes
R3	RSM	6	*B*	n/a	No
R4	RSM	2.8	*C*	Safe	Yes
R5	RSM	1.75	*C*	Unsafe	Yes

The data in Table 4 is useful to explain contradictory observations from Section 3. There, it was observed that several collapsed buildings (e.g. M1, P2 and C3) were located in the safe zone of the out-of-plane seismic index λ_o. In other words, the out-of-plane seismic index λ_o indicated that the total thickness to height ratio in these buildings should have been sufficient to resist overturning instability. However, the MQI category of these buildings are either "*C*" or "*B*" and the wall internal connection

criteria *WC* are not fulfilled ("NF"). These results indicate that leaves may have separated during the earthquakes, reducing the effective thickness of the wall in Eq.(3), and rendering it unsafe against overturning. For M1, separation of internal and external leaves can be observed in Fig.7b. This disaggregation may have been responsible for the subsequent collapse of the mosque dome (see Fig.3b). There are 11 buildings in Table 4, where the λ_o safety criteria is "Safe" (see colour coding) but disaggregation is observed.

Despite the good correlation between masonry disaggregation observations and the MQI category "*C*", it is important to note that MQI cannot be used as a predictor of damage. MQI uses empirically defined weights to combine various quality measures into a single scalar. However, as observed for M1, a specific weakness (e.g. as indicated the parameter *WC*) can lead to premature failure in walls even though all other aspects of the construction are good. This is mentioned as a limitation of the MQI approach in a recent review study, which also cites alternative construction quality indicators (Szabó et al., 2023). Furthermore, it is important to note that the incidence of disaggregation damage relates to aspects that are not considered by the MQI, such as the seismic demands on the wall and the supporting structural system. For example, the masonry quality in M5 is categorized as "*C*". However, disaggregation in this building remains limited due to comparatively low seismic demand and rigid diaphragm action offered by the RC slab and frame system connecting masonry walls.

5. In-situ material measurements

Limited samples from only a small number of buildings could be collected for destructive testing in the laboratory due to the heritage status of buildings. In the absence of laboratory samples, in-situ tests had to be conducted to quantify material properties (see (Barnaure and Cincu, 2020) for a review of typical tests). Tests involving in-situ loading (e.g. flat jack test) could not be applied due to safety concerns. Instead, the elastic modulus and compressive strength of stones were characterised using UPV and SRH measurements, and the compressive strength of mortars were estimated using MP tests. The devices and procedures used for the UPV, SRH and MP tests are discussed in the subsections 5.1.1, 5.1.2 and 5.1.3. The numerical data obtained for material properties are presented in Section 5.2. Established correlations from the literature are also used in this section to derive various other relevant material parameters (such as cohesion and friction angle of mortars) and the mechanical properties of homogenised masonry walls.

5.1. Measurement techniques

All the in-situ measurements were performed on the walls of the investigated buildings. Intact loose stones from the building debris were used for measurement when available. The SRH and UPV measurements were taken on all visually distinguishable stone types. A minimum of two stones of each type were considered to evaluate variability and up to five stone types per building were investigated. Surface and internal MP tests were performed at least from three different locations for at least two walls per building.

5.1.1. UPV measurements

UPV test makes use of the fact that ultrasonic waves propagate at different velocities through materials with varying densities and mechanical properties. By measuring the time it takes for waves to travel, wave propagation velocity can be determined. This can then be used to estimate material properties such as density (ρ_s) (Gardner et al., 1974) and dynamic elastic modulus (E_{dyn}) (Gonen and Soyoz, 2021). UPV tests are conducted using the following equipment: i) Transmitter: A transducer that generates the ultrasonic waves sent into the sample, ii) Receiver: A transducer that measures the ultrasonic waves that travelled through the stone, iii) Controller: A device for generating the electrical signals sent to the transmitter and digitising the signals from the receiver. The controller also processes the signals (using the time and distance of travel) to obtain the P-wave velocity, V_p.

When measuring stones in-situ, UPV tests were performed using indirect transmission (Fig.8a). The direct transmission technique was used when measurements were conducted on loose stones (Fig.8b). PUNDIT PL-200 testing device with 54 Hz exponential transducers were used. The exponential transducers were preferred as they can conduct measurements on rough surfaces without coupling agents (Wróblewska et al., 2021). The UPV device was calibrated regularly (e.g. when the subject wall or building changed) using the special calibration rod (see Fig.8b) to minimize measurement errors. The velocity measurements were repeated three times and averaged to obtain V_p.

(a) (b)

Fig.8. a) Indirect UPV measurement on a an in-situ stone fromR4, and b) direct UPV measurement on a disaggregated stone from C3

The following equation can be used to estimate E_{dyn} (Marazzani et al., 2021):

$$E_{dyn} = \frac{V_p^2 \rho_s (1+v_s)(1-2v_s)}{(1-v_s)10^6} \quad \text{(MPa)} \tag{5}$$

where v_s is the Poisson's ratio for the stone. The units for V_p and ρ_s in Eq.(5) are m/s and kg/m^3, respectively. It can be observed from Eq.(5) that accurate estimation of E_{dyn} requires the use of appropriate v_s and ρ_s values, in addition to measured wave velocity V_p. In the literature, the value for Poisson's ratio of different stones varies between 0.13-0.33 (Li et al., 2023; Wang et al., 2024).

It will be assumed as 0.25 in this study. Since it was not possible to measure the density of in-situ stones, empirical relations between ρ_s and V_p for natural stones were used (Gardner et al., 1974; Günaydin et al., 2022):

$$\rho_s = 230 V_p^{0.25} \qquad (\mathrm{kg/m^3}) \tag{6}$$

The accuracy of density estimation using Eq.(6) will be evaluated in Section 5.2.

The elastic modulus obtained using Eq.(5) is called "dynamic" due to the negligible strain levels during ultrasonic testing. Static elastic modulus of stones (E_{sta}) is smaller compared to E_{dyn}. Several empirical equations were presented for different type of stones to estimate E_{sta} using E_{dyn} (Eissa and Kazi, 1988; Al-Shayea, 2004; Brotons et al., 2014). In this study, Eq.(7) was chosen to calculate E_{sta} as it was derived from a large dataset featuring different stone types (Eissa and Kazi, 1988; Gonen and Soyoz, 2021).:

$$E_{sta} = 0.74 E_{dyn} - 820 \qquad (\mathrm{MPa}) \tag{7}$$

The UPV tests were conducted in different parts of the building, on in-situ and loose stones. In MLM walls, measurements were conducted on both ashlar and internal rubble stones. The results of these tests are averaged to estimate E_{sta} values for each building.

5.1.2. SRH tests

The SRH is a portable instrument used for assessing the compressive strength of masonry stones. It measures the rebound of a spring-loaded hammer after striking the surface of the material, providing an indirect estimation of its strength. In the field study, Silver SRH of Proceq is used. The Silver SRH uses optical sensors to measure the impact and rebound velocity. These velocity measurements are used to calculate the Q value. As such, the Q value is not influenced by the friction on the guide rod or the relative velocity between the unit and the specimen. It is also independent of the impact direction (Viles et al., 2011). These aspects enable the use of Silver SRH for testing in-situ and loose stones. The Silver SRH is compatible with a mushroom plunger that enables measuring compressive strengths as low as of 5 MPa (Kumavat et al., 2021).

(a) (b)

Fig.9. a) Preparing phase of a stone for SRH test in building C2 b) SRH measurement on a stone from a collapsed wall of M1

Before applying the SRH, the surface of the stones is cleaned with polishing tool (Fig.9a). Fig.9b shows the SRH test being performed on a loose stone sample. Ten readings were obtained by conducting rebound measurements in small area. Readings are averaged to obtain the Q value that is used to calculate the compressive strength of stone (f_s):

$$f_s = 0.0108Q^2 + 0.2236Q \qquad \text{(MPa)} \tag{8}$$

It should be noted that Eq.(8) is valid for Q values between 13 and 44 which corresponds to compressive strength values between 5 and 31 MPa (Kocáb et al., 2019). The procedure was applied to in-situ and loose stones to estimate an average value of f_s for each building.

5.1.3. MP tests

The MP device (see Figs.10a-b) of Diagnostic Research Company (DRC) was used to estimate the compressive strength of mortars (f_m) from the investigated buildings. The MP device has a hammer that is attached to a manually loaded spring. When released, the hammer strikes a steel needle and the mortar is exposed to dynamic blows with consistent impact energy. This energy causes the needle's tip to penetrate the mortar. According to the manufacturer's instructions, the test should be conducted by striking the needle 10 times. The penetration depth is then measured and used to calculate compressive strength of mortar with Eq.(9):

$$f_m = \frac{5970 - \sqrt{(1.58d_m - 5.3)10^6}}{1580} \qquad \text{(MPa)} \tag{9}$$

where d_m is penetration depth in mm. The equation is valid for penetrations in the range 4 to 22 mm (Gambilongo et al., 2023).

MP tests were performed both at the surface (Fig.10a-b) and internally, e.g. at an approximate depth of 8cm from the surface of the wall (Fig.10c). This was done to evaluate potential mechanical differences in mortar located in different parts of the wall. The MP tests were performed multiple times in different parts of masonry walls on site and f_m values were calculated using Eq.(9). Building-wide averages were then calculated for surface and internal measurements to obtain representative values for each structure.

(a) (b) (c)

Fig.10. a) MP test for a thin mortar between corner cut-stones b) MP test for a thick mortar between irregular rubble stones (building: C6) c) drilling of an access hole to perform an internal MP test on a thick mortar

5.2. Results and discussion

Correct estimation of E_{dyn} of stones relies on using the correct density value ρ_s in Eq.(5). Since it was not possible to measure density of stones in-situ, the use of Eq.(6) to estimate ρ_s values were proposed. Before doing this, the accuracy of Eq.(6) was evaluated by conducting gross density measurements on loose stones on site (e.g. by measuring their weight and roughly estimating their volume). This verification was performed for several samples and the results are provided in Table 5. According to the table, the maximum relative error for ρ_s is lower than 15%. This is considered acceptable since the loose stones on site were not regular and consequently the 'measured' densities were approximate.

Table 5. Comparison of ρ_s values obtained from Eq.(6) and gross density measurements performed on loose stone samples

Stone sample	Building	ρ_s (kg/m^3)		% Difference
		Measured (by weighing on site)	Estimated (by Eq.(6))	
1	C6	1994.2	2287.7	14.7
2	C9	2144.8	2427.0	13.2
3	C9	2168.4	2404.4	10.9
4	M1	2411.7	2402.6	0.4
5	M2	2168.6	2144.2	1.1
6	M2	2033.0	2101.2	3.4
7	P1	2424.1	2231.5	7.9
8	P1	1826.9	1825.7	0.1
9	P1	2035.9	2266.4	11.3
10	P1	2109.7	2200.1	4.3
11	P1	2326.5	2299.2	1.2
12	R4	2281.6	2474.7	8.5
13	R4	2424.2	2332.4	3.8

When the UPV and SRH techniques are applied to the same stones, consistent results are obtained for the elastic modulus and compressive strength; these results show the expected correlations. However, such correlations depend on the type of stones. Since chemical characterisation of stones was not possible on site, this relationship is not explored further and individual results are not plotted here for brevity. Instead, building-wide averages for the static elastic modulus and compressive strength of stones are calculated. Table 6 shows that E_{sta} and f_s values vary between 2043-15261 MPa and 13.5-31.2 MPa, respectively. Although the estimated f_s values in Table 6 for some buildings (P1, R2 and R4) are slightly higher than the limit of Eq.(8), they are still reported for completeness. The standard deviation values for the compressive strength are also provided and indicate significant variability of strength estimates in both the RSM and ISM buildings. This is not surprising considering the wide variety of stones used in the walls. The average value of f_s is obtained as 25 and 26 MPa for buildings with ISM and RSM walls. The results further indicate that systematic differences are not observed between the average compressive strength values of ashlar and rubble stones used in MLM walls (not shown).

Table 6. Estimated static elastic modulus and compressive strength of stones of the investigated buildings

Building	Wall construction	E_{sta} (MPa)	f_s (MPa) average±standard deviation
C3	RSM	8726	13.5±5.2
C4	ISM	11538	18.5±8.9
C5	RSM	7956.4	24.1±3.4
C6	ISM	10553.8	26.2±4.3
C7	ISM	14461	23.5±6.5
C8	ISM	7645.6	25.2±3.5
C9	ISM	8578	26.1±6.2
M1	RSM	15260.2	26.9±4.5
M2	RSM	3398	22.2±8.6
M3	RSM	6506	26.5±2.1
M4	RSM	11604.6	28.5±2.6
M5	ISM	6128.6	25.9±6.5
M6	RSM	2043.8	28.2±1.8
M7	RSM	5114.8	27.4±3.2
P1	RSM	7690	28.6±3.5
P2	ISM	6787.2	24.7±5.4
P3	ISM	4471	21.8±5.5
R1	RSM	8859.2	28.6±1.8
R2	RSM	8755.6	31.2±2.7
R3	RSM	8407.8	28±5.9
R4	RSM	12041.2	31±3.9
R5	RSM	10442.8	21.7±7.5

Building-wide average mortar compressive strength values obtained from surface and internal MP tests are presented in Table 7. The values range from 0.4-2.2 MPa for surface tests and 0.6-3.1 MPa for internal tests. In general, compressive strength of mortars obtained from surface and internal tests indicate different values. Sometimes, due to repointing or more carbonation, mortars are stronger on the surface. At other times, mortars are stronger inside as they are exposed less to environmental weathering. In the absence of any clear trends, it is considered appropriate to consider the average of surface and internal values to represent mortar compressive strength. The average value of f_m is 1.48 MPa for RSM constructions while the corresponding value is 1.36 MPa for ISM which indicates there is no trend for mortar quality based on wall construction type. More generally, the data indicates that further investigations on historic buildings should consider weak mortar characteristics, with a typical capacity less than 2 MPa.

Table 7. MP test results with general view and type of the historic mortars

Building	Wall construction	Measurement		
		Surface	Internal	Average
		f_m (MPa)		
C3	RSM	2.1	n/a	2.1
C4	ISM	1.2	n/a	1.2
C6	ISM	1.7	3.1	2.4

C7	ISM	2.2	0.7	1.45
C8	ISM	1.1	0.8	0.95
C9	ISM	2.2	1.8	2.0
M1	RSM	1.1	0.9	1.0
M4	RSM	1.5	2.9	2.2
M5	RSM	0.5	1.3	0.9
M6	RSM	1.5	1.2	1.35
P1	RSM	n/a	0.6	0.6
P2	ISM	0.5	n/a	0.5
P3	ISM	0.4	1.7	1.05
R1	RSM	1.3	1.0	1.15
R3	RSM	1.3	1.3	1.3
R4	RSM	2.0	2.0	2.0
R5	RSM	n/a	2.2	2.2

Average stone and mortar compressive strength values are plotted in Fig.11a. Other key parameters that may be used in numerical investigations include the cohesion (c) and the coefficient of friction of mortar (μ). c and μ were estimated using the average f_m values in Table 7 and interpolating the NZSEE recommendations (see Table 8) for non-cohesive, soft and firm historic masonry mortar properties (Ghiassi et al., 2019). The resulting values are shown in Fig.11b, where the values of c and μ vary between 0.05-0.15 MPa and 0.2-0.5, respectively.

Table 8. NZSEE recommendations (NZSEE, 2006) for mechanical properties of mortar

Type	f_m (MPa)	c (MPa)	μ
Non cohesive	0	0	0
Soft	1	0.1	0.4
Firm	4	0.2	0.6
Stiff	8	0.4	0.8

The compressive strength (f_{mas}) and elastic modulus (E_{mas}) of masonry walls are two key parameters required for the analysis homogenized masonry walls in finite element simulations. These parameters are estimated in various earthquake code of regulations using masonry constituents' strength properties. According to EC6 (2005) and TBEC2018 (2018), the f_{mas} can be calculated as follows:

$$f_{mas} = \kappa f_s^{\alpha} f_m^{\beta} \tag{10}$$

where κ, α and β are considered as 0.45, 0.7 and 0.3 for masonry made with natural stone and general purpose/light weight mortar.

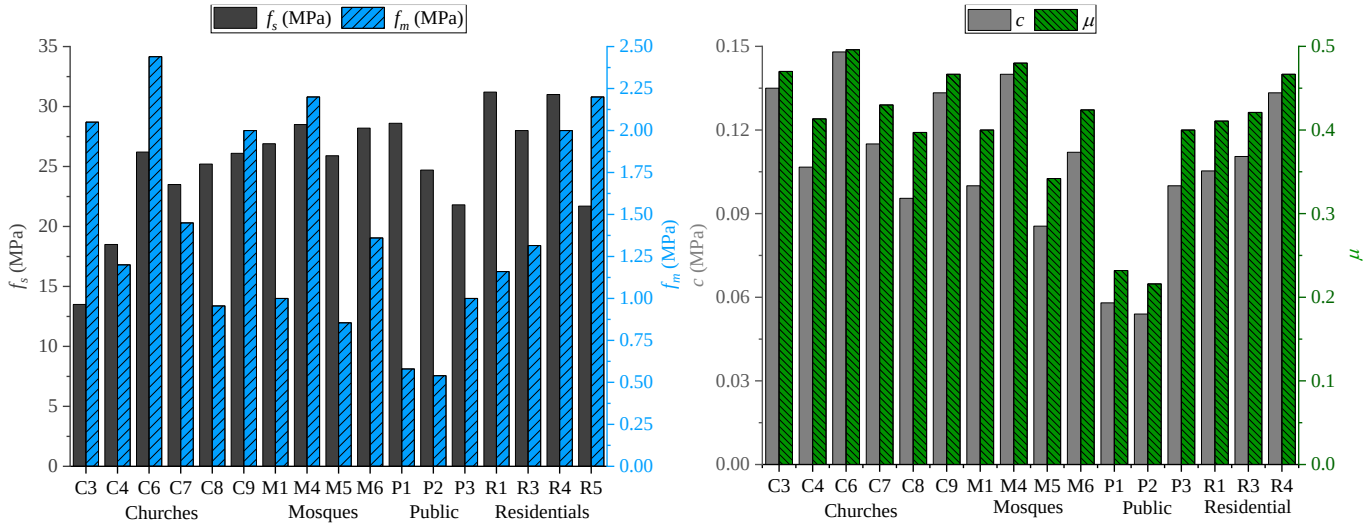

Fig.11. a) Compressive strength values for stone and mortar b) tangent of friction angle and cohesion values

The modulus of elasticity of masonry walls can be estimated using Eq.(11) where ψ is a coefficient based on correlation between f_{mas} and E_{mas} and generally varies between 300 and 1000. The EC6 and TBEC2018 consider ψ as 1000 and 750, respectively (Gonen and Soyoz, 2021).

$$E_{mas} = \psi f_{mas} \tag{11}$$

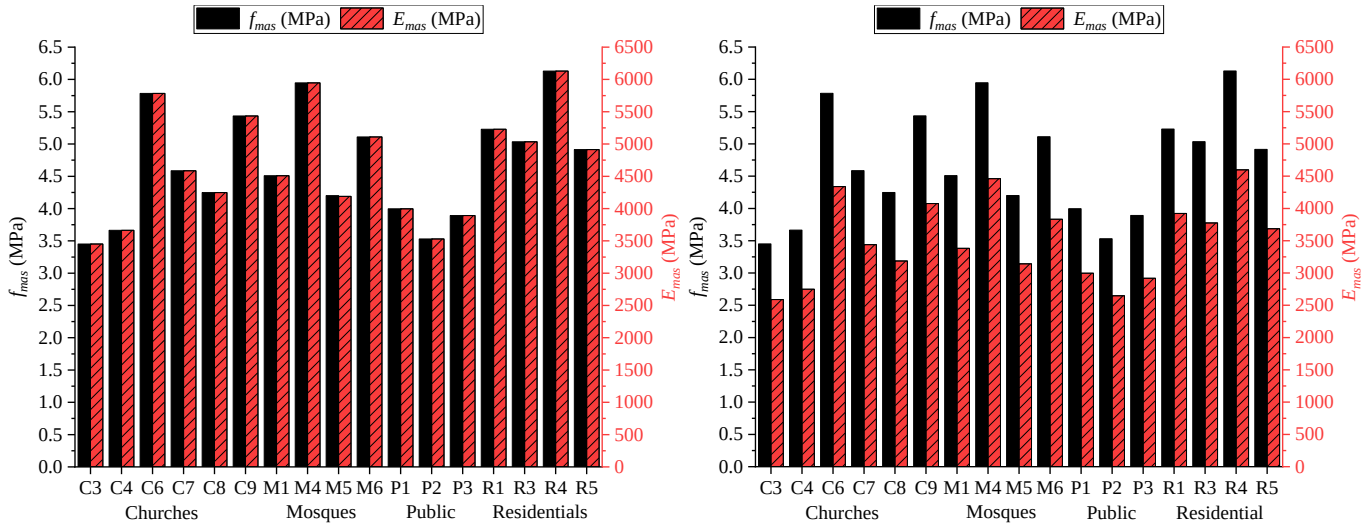

Fig.12. Compressive strength and elastic modulus values for masonry a) using EC6 equations b) using TBEC2018 equations

Using Eqs.(10-11), the f_{mas} and E_{mas} values are calculated. These are presented in Figs.12a-b for EC6 and TBEC2018. f_{mas} ranges between 3.4 and 6.2 MPa according to EC6 and TBEC2018, while E_{mas} varies between 3450-6130 MPa and 2585-4600 for EC6 and TBEC2018, respectively.

6. Conclusions

To understand the damage experienced by the monumental stone masonry buildings in Hatay and Osmaniye provinces after the 2023 Turkey-Syria earthquakes, an assessment of wall geometry and construction quality was performed. In addition, the

mechanical properties of stones and mortars used in the building walls were estimated by in-situ non-destructive material tests. Conclusions from the investigations are summarised below:

- Inspection of in-plane wall geometry indices indicate that most buildings did not have sufficient walls to resist the significant seismic demands that were experienced during the earthquakes. This deficiency may have promoted the out-of-plane failures observed in the collapsed buildings.
- The out-of-plane indices suggest that most building walls were sufficiently thick to resist the seismic demands. However, 70% of the investigated buildings experienced masonry disaggregation, which reduced the effective thickness of walls and led to out-of-plane collapse.
- According to MQI calculations, 75% of the investigated buildings are designated with class "*C*" which indicates poor masonry constructions prone to disaggregation under seismic actions. Majority of these buildings are constructed using irregular stone masonry and experienced disaggregation. Some regular masonry constructions, including those with multi-leaf walls, are characterised with poor internal connections, which explains their poor out-of-plane performance.
- In addition to poor connections, the widespread disaggregation failures indicate poor materials. In the scientific literature, there was limited information on stone masonry materials used in the region. For this reason, Ultrasonic Pulse Velocity, Schmidt Hammer and Mortar Penetrometer tests were conducted on site. The average compressive strength of stone and mortar in buildings is estimated to range between 13.5-31.2 MPa and 0.5-2.4 Mpa, respectively. This reflects the wide variety of materials used in the region and indicates poor mortar quality which may have promoted disaggregation failures, particularly in ISM walls. Using correlations from codes of guidance, the average compressive strength of masonry walls was also estimated to vary between 3.4 and 6.2 MPa. The data collected in this research also highlighted some limitations of the wall geometry and construction quality indices. These are summarised below:

- The in-plane indices correctly estimated that collapsed buildings were 'unsafe'. However, the second in-plane index indications were excessively conservative and estimated that nearly all buildings (including undamaged ones) were 'unsafe'. To achieve more useful predictions with this index, it may be necessary to consider the influence of cohesion and the weight of the building.
- In the presence of masonry disaggregation, the out-of-plane index thresholds provide unconservative assessments of safety. Future evaluations should discard the use of this index in case of disaggregation.
- The MQI category "*C*" correlated well with masonry disaggregation. However, the occurrence of masonry disaggregation depends on the local seismic demand; therefore, MQI should be seen as an indicator of disaggregation vulnerability rather than a predictive index. Furthermore, correlations between damage patterns and MQI categories indicated that specific parameters, such as wall-leaf connection, may have a dominant influence on wall behaviour. Therefore, caution should be exercised in the use of MQI overall category as a potential indicator of wall load capacity.

Damage observations from the field also indicated that aspects which have not been considered in this study (such as floor structures, progressive damage due to sequential earthquakes, soil-structure interaction and vertical ground accelerations) may have influenced building damage. To understand the influence of these aspects, computational analyses are needed, which require detailed knowledge of the mechanical properties of masonry constituents. It is hoped that the data presented in this paper will form the basis of such further investigations.

Acknowledgements

The field work conducted as a part of this study was supported by EPSRC (via the grants EP/P025641/1 and EP/V048082/1) and TUBITAK (2221-Fellowships for Visiting Scientists and Scientists on Sabbatical Leave Support Programme). Earthquake Engineering Field Investigation Team (EEFIT) organised the first field mission. Baran Bozyigit acknowledges the financial support of TUBITAK 2219-International Postdoctoral Research Fellowship Programme. The authors would like to thank Shirley Underwood from Screening Eagle/Proceq for the loan of NDT equipment used in this research. Thanks are also due to DRC Italia for supplying equipment at short notice. FARO UK provided free software licenses to enable laser scan data processing – University of Oxford DPhil students Yilong Yang, Yixiong Jing and Zheng-You Zhang provided the processed data. The authors are grateful to building owners and custodians for allowing them access; the list is too long to acknowledge here but special thanks are due to Yusuf Tabasyan (Iskenderun Karasun Manuk Church), Ratibe Bugrahan (Hatay Metropolitan Municipality) Gokhan Cicek (Directorate of Foundations), Abdullah Papas (St George Sarilar Orthodox Church) and Dimyan Emektas (St Ilyas Orthodox Church). Logistic help from Misel Uyar (Nehna) and Ahmet Cakmak (Istanbul Metropolitan Municipality) made this work possible. We also acknowledge our academic collaborators, Prof. Heather Viles, Prof. Alper Ilki, Prof. Bora Pulatsu, Prof. Eser Cakti, Prof. Paulo Lourenço and Dr Pascal Lava for contributing in various ways to this study.

References

Abrahamczyk L, Schwarz J, Langhammer T, Genes MC, Bikçe M, Kaçin S and Gülkan P (2013) Seismic risk assessment and mitigation in the Antakya–Maras region (SERAMAR): empirical studies on the basis of EMS-98. *Earthquake Spectra* 29(3): 683-704.

AFAD (2023) Turkish Ministry of Interior Disaster and Emergency Management Presidency.

Al-Shayea NA (2004) Effects of testing methods and conditions on the elastic properties of limestone rock. *Engineering geology* 74(1-2): 139-156.

Banerjee Basu S and Shinozuka M (2011) Effect of Ground Motion Directionality on Fragility Characteristics of a Highway Bridge. *Advances in Civil Engineering* 2011: 536171.

Barnaure M and Cincu M (2020) Testing methods for the assessment of material properties in historical masonry structures: a review. *IOP conference series: materials science and engineering.* IOP Publishing, 012003.

528 Borri A, Corradi M, Castori G and De Maria A (2015) A method for the analysis and classification of historic masonry. *Bulletin*
529 *of Earthquake Engineering* 13: 2647-2665.
530 Borri A, Corradi M and De Maria A (2020) The Failure of Masonry Walls by Disaggregation and the Masonry Quality Index.
531 *Heritage* 3(4): 1162-1198.
532 Brotons V, Tomás R, Ivorra S and Grediaga A (2014) Relationship between static and dynamic elastic modulus of calcarenite
533 heated at different temperatures: the San Julián's stone. *Bulletin of Engineering Geology and the Environment* 73: 791-799.
534 Demir A (2016) *Çağlar İçinde Antakya (in Turkish).* Dafne Kitap.
535 EERC (2023) *Preliminary Reconnaissance Report on February 6, 2023 Kahramanmaraş Pazarcık (Mw= .7) and Elbistan*
536 *(Mw=7.6) Earthquakes*. Middle East Technical University, Ankara.
537 Eissa EA and Kazi A (1988) Relation between static and dynamic Young's moduli of rocks. *International Journal of Rock*
538 *Mechanics and Mining Sciences* 25(6): 479-482.
539 Gambilongo L, Barontini A, Silva RA and Lourenço PB (2023) Evaluation of non-destructive techniques for mechanical
540 characterisation of earth-based mortars in masonry joints. *Construction and Building Materials* 392: 131960.
541 Garbioğlu Ö (2017) *Tanzimat'tan Cumhuriyet'e Hatay'daki Kamu Yapıları. Master's Thesis (in Turkish)*. Mimar Sinan Fine Art
542 University.
543 Gardner G, Gardner L and Gregory A (1974) Formation velocity and density—The diagnostic basics for stratigraphic traps.
544 *Geophysics* 39(6): 770-780.
545 Geneş MC, Abrahamczyk L, Kaçın S and Erberik MA (2017) Yığma yapıların deprem etkisi altında gözleme ve hesaba bağlı
546 değerlendirilmesi için yöntem (in Turkish). In: *4.UDMSK*.
547 Ghiassi B, Vermelfoort AT and Lourenço PB (2019) Chapter 7 - Masonry mechanical properties. In: Ghiassi B and Milani G
548 (eds) *Numerical Modeling of Masonry and Historical Structures*. Woodhead Publishing, pp.239-261.
549 Gonen S and Soyoz S (2021) Investigations on the elasticity modulus of stone masonry. *Structures.* Elsevier, 378-389.
550 Grünthal G and Levret A (1998) European macroseismic scale 1998 (EMS-98) cahiers du centre Européen de géodynamique et
551 de séismologie 15. *Centre Européen de géodynamique et de séismologie, Luxembourg*.
552 Günaydin M, Genç AF, Altunışık AC, Haciefendioğlu K, Okur FY, Okur E and Adanur S (2022) Structural condition assessment
553 of a historical masonry school building using experimental and numerical methods. *Journal of Civil Structural Health*
554 *Monitoring* 12(5): 1083-1113.
555 Housner GW (1963) The behavior of inverted pendulum structures during earthquakes. *Bulletin of the Seismological Society of*
556 *America* 53(2): 403-417.
557 Karabacak V, Özkaymak Ç, Sözbilir H, Tatar O, Aktuğ B, Özdağ ÖC, Çakir R, Aksoy E, Koçbulut F and Softa M (2023) The
558 2023 Pazarcık (Kahramanmaraş, Türkiye) earthquake (Mw 7.7): implications for surface rupture dynamics along the East
559 Anatolian Fault Zone. The Geological Society of London, jgs2023-2020.

Kocáb D, Misák P and Cikrle P (2019) Characteristic curve and its use in determining the compressive strength of concrete by the rebound hammer test. *Materials* 12(17): 2705.

Kumavat HR, Chandak NR and Patil IT (2021) Factors influencing the performance of rebound hammer used for non-destructive testing of concrete members: A review. *Case Studies in Construction Materials* 14: e00491.

Li H, Yang S-Q, Yang Z, Zhou X-P, Tian W-L and Wang S-S (2023) Experimental and numerical study on the mechanical behaviors and crack propagation of sandstone containing two parallel fissures. *Theoretical and Applied Fracture Mechanics* 126: 103965.

Lourenço PB, Oliveira DV, Leite JC, Ingham JM, Modena C and da Porto F (2013) Simplified indexes for the seismic assessment of masonry buildings: International database and validation. *Engineering Failure Analysis* 34: 585-605.

Lourenço PB and Roque JA (2006) Simplified indexes for the seismic vulnerability of ancient masonry buildings. *Construction and Building Materials* 20(4): 200-208.

Marazzani J, Cavalagli N and Gusella V (2021) Elastic properties estimation of masonry walls through the propagation of elastic waves: An experimental investigation. *Applied Sciences* 11(19): 9091.

Mavroulis S, Andreadakis E, Spyrou N-I, Antoniou V, Skourtsos E, Papadimitriou P, Kasssaras I, Kaviris G, Tselentis GA, Voulgaris N, Carydis P and Lekkas E (2019) UAV and GIS based rapid earthquake-induced building damage assessment and methodology for EMS-98 isoseismal map drawing: The June 12, 2017 Mw 6.3 Lesvos (Northeastern Aegean, Greece) earthquake. *International Journal of Disaster Risk Reduction* 37: 101169.

NZSEE (2006) Assessment and Improvement of the Structural Performance of Buildings in Earthquakes. *New Zealand Society for Earthquake Engineering*.

Ozturk M, Arslan MH and Korkmaz HH (2023) Effect on RC buildings of 6 February 2023 Turkey earthquake doublets and new doctrines for seismic design. *Engineering Failure Analysis* 153: 107521.

Över S, Büyüksaraç A, Bekta Ö and Filazi A (2011) Assessment of potential seismic hazard and site effect in Antakya (Hatay Province), SE Turkey. *Environmental Earth Sciences* 62(2): 313-326.

Sagbas G, Sheikhi Garjan R, Sarikaya K and Deniz D (2023) Field reconnaissance on seismic performance and functionality of Turkish industrial facilities affected by the 2023 Kahramanmaras earthquake sequence. *Bulletin of Earthquake Engineering*. DOI: 10.1007/s10518-023-01741-8.

Sanci F (2006) *Hatay İlinde Türk Mimarisi I. Doctoral Thesis (in Turkish)*. Ankara University.

Standardization ECf (2005) *Eurocode 6: Design of Masonry Structures – Part 1-1: General rules for reinforced and unreinforced masonry structures.*

Sürmeli BS (2019) *Hatay Musa Dağı kırsal yerleşimleri ve geleneksel konutların korunması için öneriler. Master's Thesis (in Turkish)*. Istanbul Technical University.

591 Szabó S, Funari MF and Lourenço PB (2023) Masonry patterns' influence on the damage assessment of URM walls: Current
592 and future trends. *Developments in the Built Environment* 13: 100119.
593 TAÇDAM (2023) *Antakya'nın Çok Katmanlı Kültürel Mirasının Deprem Sonrası Belgelenmesi, Hasar Tespiti ve*
594 *Değerlendirilmesi (in Turkish)*. Middle East Technical University, Ankara.
595 Taftsoglou M, Valkaniotis S, Papathanassiou G and Karantanellis E (2023) Satellite Imagery for Rapid Detection of Liquefaction
596 Surface Manifestations: The Case Study of Türkiye–Syria 2023 Earthquakes. *Remote Sensing* 15(17): 4190.
597 TBEC (2018) Turkish Building Earthquake Code. *Turkish Ministry of Interior Disaster and Emergency Management Presidency,*
598 *Ankara.*
599 USGS (2023) U.S. Geological Survey. *Earthquake Lists, Maps, and Statistics, accessed July 13, 2023 at URL*
600 *https://www.usgs.gov/natural-hazards/earthquake-hazards/lists-maps-and-statistics*.
601 Viles H, Goudie A, Grab S and Lalley J (2011) The use of the Schmidt Hammer and Equotip for rock hardness assessment in
602 geomorphology and heritage science: a comparative analysis. *Earth surface processes and landforms* 36(3): 320-333.
603 Wang X, Cheng Z, Zhou Y, Xu K and Liao Y (2024) Study on microscopic failure mechanism and numerical simulation of
604 sandstone under different saturated pressure. *Unconventional Resources* 4: 100058.
605 Wróblewska J, Kowalski R, Głowacki M and Juchnowicz-Bierbasz B (2021) Application of ultrasonic pulse velocity test to
606 concrete assessment in structures after fire. *Archives of Civil Engineering* 67(3): 395-413.

607